Received: 20 August 2021 | Revised: 8 February 2022 | Accepted: 12 February 2022

DOI: 10.1111/nan.12812

ORIGINAL ARTICLE

Neuropathology and Applied Neurobiology
JOURNAL OF THE BRITISH NEUROPATHOLOGICAL SOCIETY

WILEY

Neuron types in the primate striatum: Stereological analysis of projection neurons and interneurons in control and parkinsonian monkeys

Natalia López-González del Rey[1,2,3] | Inés Trigo-Damas[1,2] | José A. Obeso[1,2] | Carmen Cavada[3,4] | Javier Blesa[1,2]

[1]HM CINAC (Centro Integral de Neurociencias Abarca Campal), Hospital Universitario HM Puerta del Sur, HM Hospitales, Madrid, Spain

[2]CIBERNED (Center for Networked Biomedical Research on Neurodegenerative Diseases), Instituto Carlos III, Madrid, Spain

[3]PhD Program in Neuroscience Autónoma de Madrid University–Cajal Institute, Madrid, Spain

[4]Department of Anatomy, Histology and Neuroscience, School of Medicine, Autónoma de Madrid University, Madrid, Spain

Correspondence
Javier Blesa, HM CINAC (Centro Integral de Neurociencias Abarca Campal), Hospital Universitario HM Puerta del Sur, HM Hospitales, Madrid, Spain.
Email: jblesa.hmcinac@hmhospitales.com

Funding information
Instituto de Salud Carlos III, Grant/Award Numbers: FIS PI20/00496, Miguel Servet CP19/00200; Ministerio de Educación y Formación Profesional, Grant/Award Number: PID2019-111045RB-100; Fundación Tatiana Pérez de Guzmán el Bueno; Comunidad de Madrid, Grant/Award Number: S2017/BMD-3700

Abstract

Aims: The striatum is mainly composed of projection neurons. It also contains interneurons, which modulate and control striatal output. The aim of the present study was to assess the percentages of projection neurons and interneuron populations in the striatum of control monkeys and of parkinsonian monkeys.

Methods: Unbiased stereology was used to estimate the volume density of every neuron population in the caudate, putamen and ventral striatum of control monkeys and of monkeys treated with MPTP, which results in striatal dopamine depletion. The various neuron population phenotypes were identified by immunohistochemistry. All analyses were performed within the same subjects using similar processing and analysis parameters, thus allowing for reliable data comparisons.

Results: In control monkeys, the projection neurons, which express the dopamine-and-cAMP-regulated-phosphoprotein, 32-KDa (DARPP-32), were the most abundant: ~86% of the total neurons counted. The interneurons accounted for the remaining 14%. Among the interneurons, those expressing calretinin were the most abundant (Cr+: ~57%; ~8% of the total striatal neurons counted), followed those expressing Parvalbumin (Pv+: ~18%; 2.6%), dinucleotide phosphate-diaphorase (NADPH+: ~13%; 1.8%), choline acetyltransferase (ChAT+: ~11%; 1.5%) and tyrosine hydroxylase (TH+: ~0.5%; 0.1%). No significant changes in volume densities occurred in any population following dopamine depletion, except for the TH+ interneurons, which increased in parkinsonian non-symptomatic monkeys and even more in symptomatic monkeys.

Conclusions: These data are relevant for translational studies targeting specific neuron populations of the striatum. The fact that dopaminergic denervation does not cause neuron loss in any population has potential pathophysiological implications.

KEYWORDS
calretinin, cholinergic, DARPP-32, nitrergic, parvalbumin, tyrosine hydroxylase

INTRODUCTION

The striatum is the largest nucleus of the basal ganglia. It is involved in motor control, compulsive behaviour and habit formation [1]. The striatum is mainly composed of projection neurons, the medium spiny neurons, which are GABAergic and express the dopamine-and-cAMP-regulated-phosphoprotein, 32-KDa (DARPP-32) [2, 3]. In addition, the striatum contains a small population of interneurons which modulate striatal output [4–6]. Most interneurons are GABAergic; they are divided into several types based on their immunostaining for various proteins such as parvalbumin (Pv), calretinin (Cr), neuropeptide Y/somatostatin/nicotinamide adenine dinucleotide phosphate-diaphorase (NADPH) and tyrosine hydroxylase (TH). There is an additional, non-GABAergic, interneuron type, consisting of cholinergic interneurons that express the enzyme choline acetyltransferase (ChAT) [4, 5]. Specific interneuron circuits and functions are selectively engaged by different corticostriatal, thalamostriatal and other afferent inputs (3–8) [7–10]. Recent evidence indicates that there are highly selective interactions between projection neurons and interneuron types, as well as among interneurons themselves, that have specific functional impact on striatal networks [11–17]. Moreover, striatal interneurons are highly involved in striatal disorders, such as Parkinson's disease (PD), Huntington's disease or drug addiction [18–22]. Currently, emerging studies propose that modification of different interneuron populations could provide therapeutic approaches for those conditions [23–26].

Most information on the neuron populations of the striatum has been gathered in rodents [27, 28]. Regarding the primate striatum, there is just fragmented evidence on specific interneuron populations [27, 29]. Altogether, the population of interneurons appears higher in the primate striatum (6–26%) [27, 29–32], including the human striatum (10–26%) [28, 30–34], than in the rodent striatum (3–5%) [27, 30]. These data have been gathered in experimental studies that differ widely in the methods and variables studied, ranging from nuclear identity or dendritic features to cytosol immunostaining with diverse specificities for interneuron populations, to single-nucleus RNA sequencing.

A consistent, comprehensive and state of the art study is needed to clarify the ratios of projection neurons and interneurons in the primate striatum [28]. Here, we have used unbiased stereological methods to estimate the numerical density of diverse neuron populations in the whole extension of the striatum of control macaque monkeys and monkeys treated with 1-methyl-4-phenyl-1,-2,3,6-tetrahydropyridine (MPTP) to induce parkinsonism in various stages. The populations studied include neurons expressing DARPP-32, Cr, Pv, NADPH, ChAT and TH; the NADPH population encompasses neurons expressing somatostatin and neuropeptide Y [5, 35]. All assessments were performed within the same subjects, and using similar processing conditions and analysis parameters, thus allowing for sound comparisons among neuron populations. The data obtained are relevant in translational studies targeting specific neuron populations of the striatum. Also, the data from the MPTP-treated monkeys with different degrees of dopamine (DA) loss [36–39] are important to understand how striatal circuits adapt in the parkinsonian condition [40].

Key Points

- The primate striatum contains more interneurons than the rodent striatum.
- Among interneurons, the calretinin interneurons are the most abundant and the tyrosine hydroxylase interneurons the least.
- Dopamine depletion results in no significant density changes in any striatal neurons, except for the TH+ interneurons.

MATERIALS AND METHODS

Brain tissue

Brain tissue from our macaque monkey brain bank, described in detail in previous publications, was used [36–38, 41]. All the studies were performed according to European and Spanish guidelines (86/609/EEC and 2003/65/EC European Council Directives; and Spanish Government) and were approved by the Committees for Research Ethics of the University of Navarra and Autónoma de Madrid University.

Four macaques (*Macaca fascicularis*) were used as controls. Sixteen macaques were treated with MPTP (0.5 mg/kg, i.v.) following a slow protocol (doses every 2 weeks) [39]. Motor signs were assessed by the research team using the validated Kurlan motor score after each MPTP dose and while the parkinsonian syndrome was progressing until complete stabilisation (range, 0–29 points) [42]. Macaques that exhibited evident parkinsonian signs after the last MPTP injection and that remained affected thereafter until sacrificed were classified as symptomatic ($n = 8$; Kurlan score: 9–22). Macaques that maintained normal motor features after the second MPTP dose or those that developed transient mild parkinsonian signs but recovered and exhibited normal motor function for several weeks before sacrifice were considered non-symptomatic ($n = 8$; Kurlan score: 0) (see Table S1). The DA striatal depletion and cell loss in the *substantia nigra compacta* ranged from 40–60% reduction with respect to controls in the non-symptomatic group to 70–85% reduction in the symptomatic group [37]. None of them received L-DOPA or DA agonists during the experiment. Thus, the experimental design allowed us to ascertain the impact of different degrees of striatal dopaminergic depletion onto striatal neuron populations, mimicking to some extent what occurs throughout the evolution of PD.

Brain processing and histological staining

Monkeys were anaesthetized deeply with sodium pentobarbital (10 mg/kg, i.p.) and perfused through the ascending aorta with saline, followed by 4% paraformaldehyde in phosphate buffer and a series of phosphate buffer sucrose solutions (5–10–20%). The brains were

dissected in the midline; one hemisphere was blocked in the coronal stereotaxic plane (plane 0 corresponding to the interaural plane) and sectioned (40 μm) on a freezing microtome.

Parallel series of sections were processed to reveal the cytoarchitecture and chemoarchitecture using cresyl violet staining and acetylcholinesterase histochemistry, respectively. Acetylcholinesterase histochemistry was performed following a protocol described elsewhere [43]. These series were used to identify the striatal territories and trace their boundaries. Adjacent additional series for each marker were immunostained for DARPP-32, Cr, Pv, ChAT and TH or processed histochemically to reveal NADPH-containing neurons. This battery of antibodies in Table 1 was selected in order to mark independent, non-overlapping neuron populations. DARPP-32 in the striatum is just expressed in projections neurons [44, 45]. The remaining markers reveal specific interneuron populations. A total of seven rostro-caudal sections for each marker, regularly spaced 2400 μm apart, were studied in each monkey. Three sections were rostral and four sections caudal to the level where the anterior commissure crosses the midline (pre-commissural and post-commissural sections, respectively) (Figure 1). No significant volumes of striatal tissue were present at positions 2400 μm more rostral or more caudal than the sections selected except for the caudate tail, which is more caudal and ventral, and was not analysed in this study. All sections were processed simultaneously in all the animals for each marker.

Free-floating immunohistochemistry was performed using the primary antibodies and the secondary biotinylated antibodies shown in Table 1. Development of the immunoreaction was done using diaminobenzidine as substrate. All experimental immunohistochemistry sessions were run including control sections where the primary antibody was absent. For NADPH histochemistry, we followed the protocol described in Hope and Vincent [46].

Stereological analysis of striatal neuron densities

Immunostained neuron bodies were counted in all immunoprocessed sections (Figure 1) from all monkeys (see Sections 2.1 and 2.2) within each region of interest (caudate, putamen and ventral striatum) by means of the optical dissector, an unbiased stereological technique. We used the *StereoInvestigator* software (Version 2017.00.9, MicroBrightField, Williston, VT, USA) linked to a Zeiss Axioskop optical microscope (Oberkochen, Germany) equipped with a digital camera (AxioCam HRc, Zeiss, Germany). The motorised stage and the interactive optical dissector grids were controlled by the *StereoInvestigator* software. The regions of interest were delineated with a 2.5× objective. Grids of 380 × 380 μm were used for Cr+, Pv+ and NADPH+ interneurons; 250 × 250 μm grids were used for TH+ interneurons; and 1200 × 1200 μm grids were used for DARPP-32+ projection neurons. These sampling parameters were established following pilot studies to ensure at least 100 hits per cell type in each subject. The dimensions of the counting frames were 120 × 120 μm. Counting was performed with a 40× objective. Neuron somata were the counting unit. All parameters were set to reach error coefficients below 0.10 (Gundersen, m = 1). Error coefficients of the estimates were calculated for each brain [47, 48]. All values were below 0.1.

Numerical densities per area were calculated using the following formula [49] for all neuron populations examined:

$$N_a = \frac{\Sigma Q}{(a \cdot \Sigma P)}$$

where Q is the number of counting units in a region of interest, a is the area of the dissector and P is the number of dissectors included in the region of interest. Thus, the formula gives the number of particles in the sampled area.

Tissue shrinkage is an important issue that should be considered when comparing different immunostaining techniques. Post-mortem material may swell or shrink differently depending on fixation, sectioning and staining protocol, and this can affect the estimation of numerical densities. In this study, all the sections were from the same subjects and treated in the same way from brain extraction to storage after sectioning. Differential shrinkage could happen mostly after sectioning during each specific staining protocol. In order to discard post-sectioning thickness differences among the various processing

TABLE 1 Antibodies used for histological techniques

Marker	Host animal	Reference	Dilution
Primary antibodies			
Polyclonal anti-DARPP-32	Rabbit	AB10518, Millipore	1:400
Monoclonal anti-Cr	Mouse	6B3, Swant	1:2500
Monoclonal anti-Pv	Mouse	PV235, Swant	1:2500
Polyclonal anti-ChAT	Goat	AB144P, Millipore	1:500
Monoclonal anti-TH	Mouse	MAB5280, Chemicon	1:1000
Secondary antibodies			
Biotinylated anti-mouse	Goat	115-065-003, Jackson	1:400
Biotinylated anti-rabbit	Goat	AP132B, Chemicon	1:400
Biotinylated anti-goat	Rabbit	AP106B, Chemicon	1:500

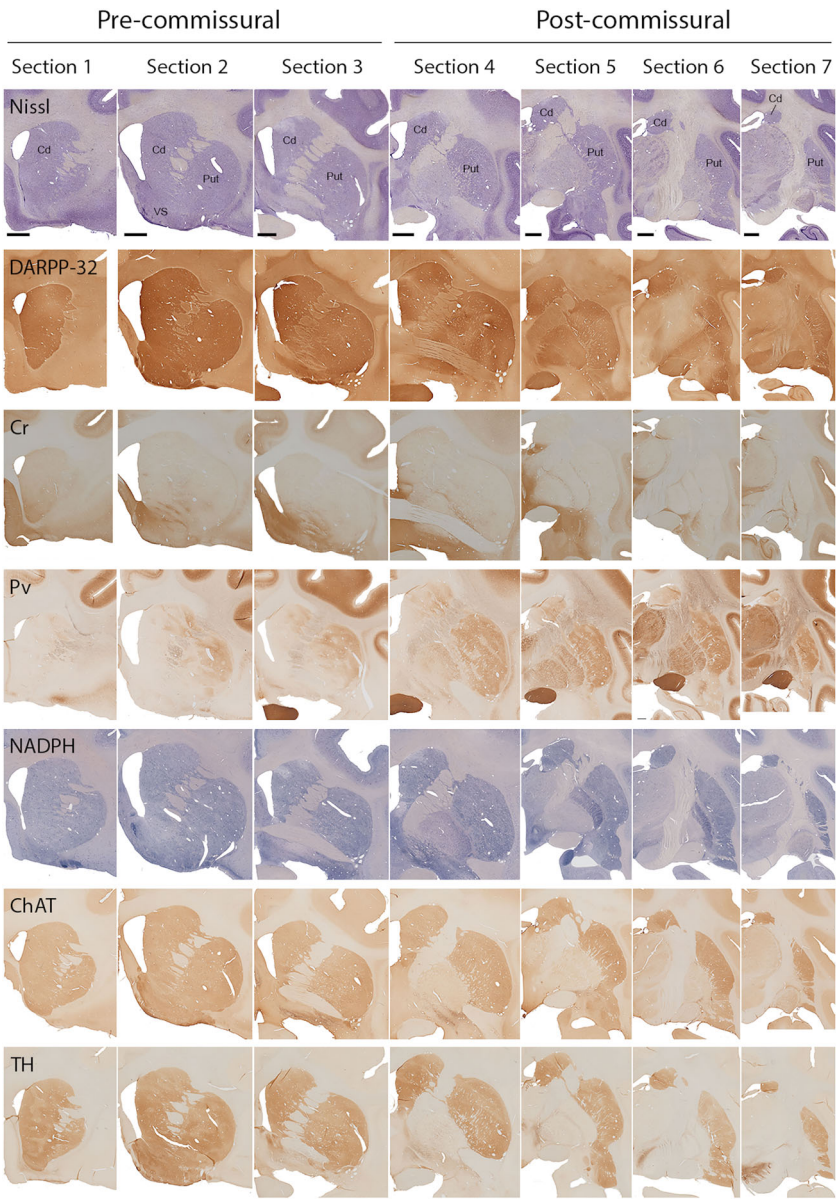

FIGURE 1 Anteroposterior low power images from a control monkey showing the staining for all markers used. Sections are evenly spaced (2400 μm apart), pre-commissural ones (sections 1–3) are anterior to the level where the anterior commissure is in the midline; post-commissural (sections 4–7) sections are posterior to this level. Scale bar = 2 mm. Pictures in each column are at the same magnification

protocols, the section thickness used to cut the brain blocks (40 μm) was considered in the formula to calculate total neuron numbers [50]. In conclusion, numerical densities per volume, corrected for Z-axis shrinkage, were calculated with the following equation [51]:

$$N_V = \frac{\Sigma Q}{(40 \cdot a \cdot \Sigma P)}$$

All data are expressed as neurons per mm^3.

In order to verify if striatal volume differences were present between animals, groups or processing protocols, the total striatal volume for each monkey was calculated with the Cavalieri method using the *StereoInvestigator* software. No differences were found. Thus, the N_v densities obtained can be reliably compared between experimental groups and processing protocols.

To get the percentages of each neuron population studied, N_v from all neuron populations were added, obtaining a total number. Then, the percentage of each neuron population was calculated.

Statistics

All data are expressed as the mean ± standard error of mean (SEM).

Statistics were performed between data from the control group and the MPTP-treated groups using the *Statistica* 12 software (StatSoft Inc., Dell Software). Data normality was checked with the Kolmogorov–Smirnov test. The striatal neuron densities were analysed using one-way ANOVA followed by Bonferroni post hoc. The significant threshold was $p < 0.05$. Graphs were made with *GraphPad Prism* 6.01 (GraphPad® Software).

Size and morphology of striatal neurons

The cell body diameters of all neuron types were assessed in two representative sections (one pre-commissural and one post-commissural) from two control monkeys. The "quick measure line" tool of the *StereoInvestigator* software was used to measure the length of the longest and shortest diameters of each cell body. One hundred eighty neurons of each neuron type from dorsolateral and ventromedial regions of the caudate and putamen and from the ventral striatum were analysed for each monkey. Data are shown in Table 2 as the mean of both the longest and shortest diameters orthogonally positioned on each neuron body.

Pictures of each striatal neuron type were taken using 4×, 10× and 40× objectives. The 4× pictures were used to build, with *Adobe Photoshop 2020 software* (version 21.01), the mosaics shown in Figure 1. The pictures taken with the 10× and 40× objectives are shown in Figures 3 through 8.

RESULTS

Percentages of projection neurons and interneurons in the primate striatum

We refer the percentage of each population to the total number of neurons counted, which includes all those expressing DARPP-32, Cr, Pv, NADPH, ChAT and TH.

In control animals ($n = 4$), the projection neurons (DARPP-32+) were the most abundant neuron type in the striatum: they account for ~86% of the total striatal population counted. Interneurons made the remaining 14% (Figure 2A). Among the interneurons, Cr+ neurons were the most abundant type (57.09%; 7.9% of the total), followed by Pv+ neurons (18.24%; 2.6% of the total), NADPH+ interneurons (13.09%; 1.8% of the total) and ChAT+ interneurons (11.04%; 1.5% of the total). The least abundant interneuron type was that expressing TH (0.54%; 0.1% of the total) (Figure 2B).

In the MPTP-treated monkeys, the percentages of each striatal neuron type were overall similar to those in control monkeys, in both the non-symptomatic and symptomatic groups (Figure 2C–F). The only exception was the population of TH+ neurons, whose percentage doubled in the MPTP-treated monkeys (Figure 2B,D,F), and which increased at any stage of nigro-striatal lesion. This is further described below. The following sections describe the main qualitative and quantitative features of each neuron type.

DARPP-32+ neurons in control and MPTP-treated monkeys

The perikaryon staining of the DARPP-32+ neurons was homogeneous. The soma of these neurons was oval with diameters of 11 μm and 7 μm (longest and shortest, respectively). DARPP-32+ neurons were mostly unipolar, but occasionally they presented two or three principal dendrites (Figure 3A,B, Table 2). The distribution and staining patterns of DARPP-32+ neurons were homogeneous throughout the whole striatum (Figure 1, Table 2).

Neuron densities of DARPP-32+ neurons were similar in the caudate (21,743 ± 420), putamen (20,784 ± 312) and ventral striatum

TABLE 2 Morphological features of each striatal neuron population

Neuron population	Perikaryal staining	Diameter μm[a]	Soma morphology	Dendrites
DARPP-32	Homogeneous, predominantly in the perikaryon	10.8 (longest) 7.3 (shortest)	Oval	Mostly unipolar, 2–3 principal dendrites occasionally
Cr	Intense or medium	10.3 (longest) 7 (shortest)	Oval and triangular	Variable dendritic fields: unipolar or multipolar (2–3 principal dendrites can be identified)
	Very light	23 (longest) 15 (shortest)	Big and oval	No dendrites visible
Pv	Intense	11.1 (longest) 7.5 (shortest)	Oval	Bipolar or multipolar
NADPH	Homogeneous and intense in the soma	15.1 (longest) 9 (shortest)	Oval	Bipolar or multipolar. Occasionally unipolar. The multipolar neurons, generally with 3 principal dendrites
ChAT[b]	The staining was present within the soma and the nuclei	22.8 (longest) 14.4 (shortest)	Polygonal	Multipolar neurons with 4–6 principal dendrites
TH	Intense	9.4 (longest) 6.13 (shortest)	Oval or round	Unipolar or bipolar neurons

[a]The longest and shortest diameters are given ($n = 180$ neurons/monkey).
[b]ChAT+ neurons were counted within the intrastriatal parenchyma (ChAT+ neurons present in the white matter adjacent to the striatum were not assessed).

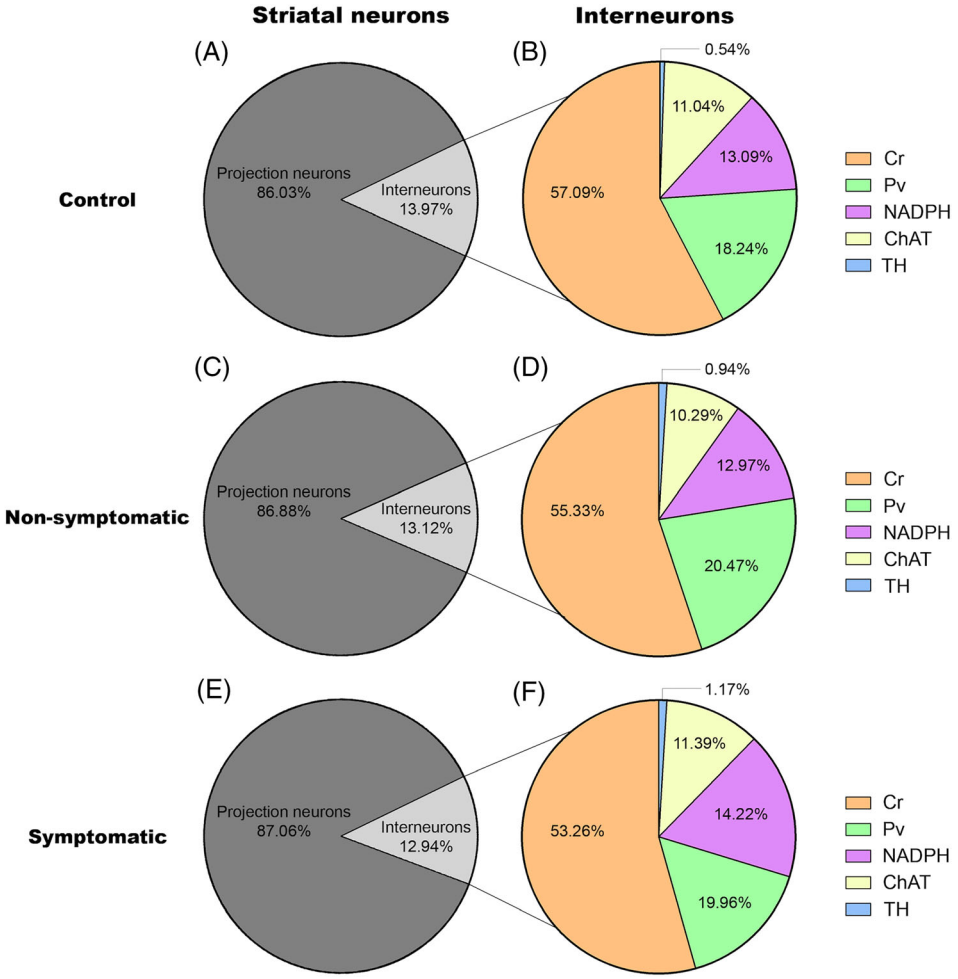

FIGURE 2 Percentages of striatal neurons in control and MPTP-treated monkeys. (A, C and E) the relative percentages of DARPP-32-projection neurons vs interneurons in the three animal groups. (B, D and F) the relative percentages of each interneuron population

(24,317 ± 1745) of control monkeys (Figure 3C). Also, densities of DARPP-32+ neurons were similar in the control and MPTP-treated groups throughout the whole striatum (control 21,154 ± 282; non-symptomatic 20,538 ± 460; symptomatic 21,449 ± 546) ($p = 0.3957$) (Figure 3C–E).

Cr+ neurons in control and MPTP-treated monkeys

The Cr+ cells were the most abundant type of striatal interneuron (Figure 2). They had different sizes and staining intensities. Two types of Cr+ neurons were identified based on their size: large and medium sized. The large Cr+ neurons were very lightly stained and quite scarce (1.3% of total Cr+ neurons in control monkeys, 1.6% in the MPTP-treated monkeys and 1.5% in the 20 monkeys studied), devoid of stained dendrites and with hard-to-define boundaries; they had the largest perikaryon, with diameters of 23 μm and 15 μm (longest and shortest, respectively) (Table 2). The large Cr+ neurons are present mostly in ventromedial regions of the putamen. The medium-sized Cr + neurons showed intense or medium immunostaining (Figure 4B); they had diameters of 10 μm and 7 μm (longest and shortest, respectively). They were oval or triangular and had variable dendritic fields, either unipolar or multipolar with two or three principal dendrites (Table 2, Figure 4A,B).

Overall, Cr staining, including Cr+ cell bodies and neuropil, was uneven throughout the striatum: The ventral striatum and ventromedial regions of the caudate head were more intensely stained than dorsolateral and caudal striatal territories (Figure 1).

There was a higher density of Cr+ interneurons in the caudate (2701 ± 353) than in the putamen (1492 ± 285) and the ventral striatum (1837 ± 187) in control monkeys (Figure 4C). This pattern was also present in the MPTP-treated monkeys (Figure 4C). Densities of Cr+ neurons were similar in the control and MPTP-treated groups throughout the whole striatum (control 1961 ± 297; non-symptomatic 1716 ± 96; symptomatic 1747 ± 110) ($p = 0.5355$) (Figure 4C–E).

Pv+ neurons in control and MPTP-treated monkeys

Pv+ interneurons had average diameters of 11 μm and 8 μm (longest and shortest, respectively). Most of them had an oval soma and highly stained dendrites. Some Pv+ neurons, with oval or polygonal somata, had long, well stained dendrites, ranging from three to five principal dendrites (Table 2, Figure 5A,B).

Overall, Pv+ staining in the striatum had a clear dorsoventral and rostrocaudal gradient complementary to the Cr+ staining: The most posterior and dorsal striatal regions were more stained than the

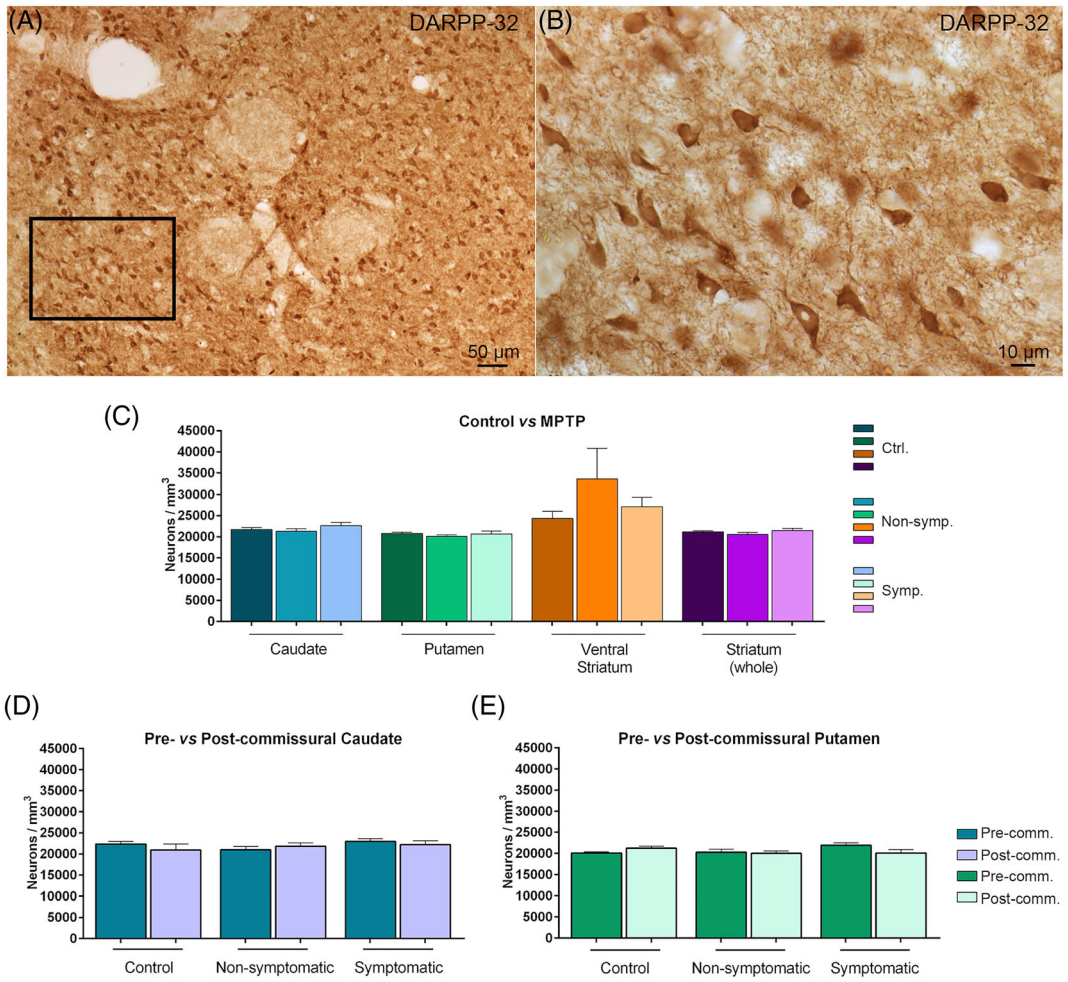

FIGURE 3 DARPP-32+ neurons. (A and B) low magnification (10×) (A) and high magnification (40×) (B) photomicrographs of neurons expressing DARPP-32 in a control monkey. The picture in (B) corresponds to the rectangle area in (A). (C) Densities of DARPP-32+ neurons in the striatal nuclei of control and MPTP-treated monkeys; and densities in pre- and post-commissural caudate (D) and putamen (E) in each experimental group. No changes in DARPP-32+ neuron densities were present in the various striatal territories of the MPTP-treated groups as compared with the control group

anterior and ventral regions. Overall, the putamen had higher levels of staining than the caudate. Also, lightly stained Pv+ patches were observed throughout the striatum; they were more defined in the putamen (Figures 1 and 5A). The reduction in Pv+ staining in the patches resulted from lighter neuropil staining as compared with the surrounding neuropil (Figure 5A).

There was a lower density of Pv+ neurons in the ventral striatum (247 ± 80) than in the caudate (583 ± 92) and putamen (659 ± 69) of control monkeys (Figure 5C). This pattern was also present in the MPTP-treated monkeys (Figure 5C). Overall, Pv+ neuron densities were higher in the post-commissural regions both in caudate (control pre-commissural caudate 412 ± 83; control post-commissural caudate 908 ± 114) and putamen (control pre-commissural putamen 503 ± 45; control post-commissural putamen 749 ± 83) nuclei (Figure 5D–E). Densities of Pv+ neurons were similar in the control and MPTP-treated groups throughout the whole striatum (control 626 ± 76; non-symptomatic 635 ± 60; symptomatic 636 ± 53) ($p = 0.9945$) (Figure 5C–E).

NADPH+ neurons in control and MPTP-treated monkeys

NADPH+ neurons had average diameters of 15 µm and 9 µm (longest and shortest, respectively). These nitrergic interneurons had oval or polygonal perikarya, which were homogeneously and intensely stained. NADPH+ neurons had two to four principal dendrites, most had three dendrites; occasional unipolar neurons were present (Table 2, Figure 6A,B).

The overall NADPH+ staining was homogeneous throughout the striatal nuclei both in the rostrocaudal and dorsoventral axes. Some patches were less stained, due to less neuropil staining, mainly in the caudate nucleus (Figure 1).

Interestingly, there was a higher density of NADPH+ neurons in the ventral striatum (609 ± 70) than in the caudate (506 ± 7) and putamen (414 ± 16) of control monkeys (Figure 6C). This pattern was also present in the MPTP-treated monkeys (Figure 6C). NADPH+ neuron densities were similar in the control and MPTP-treated groups

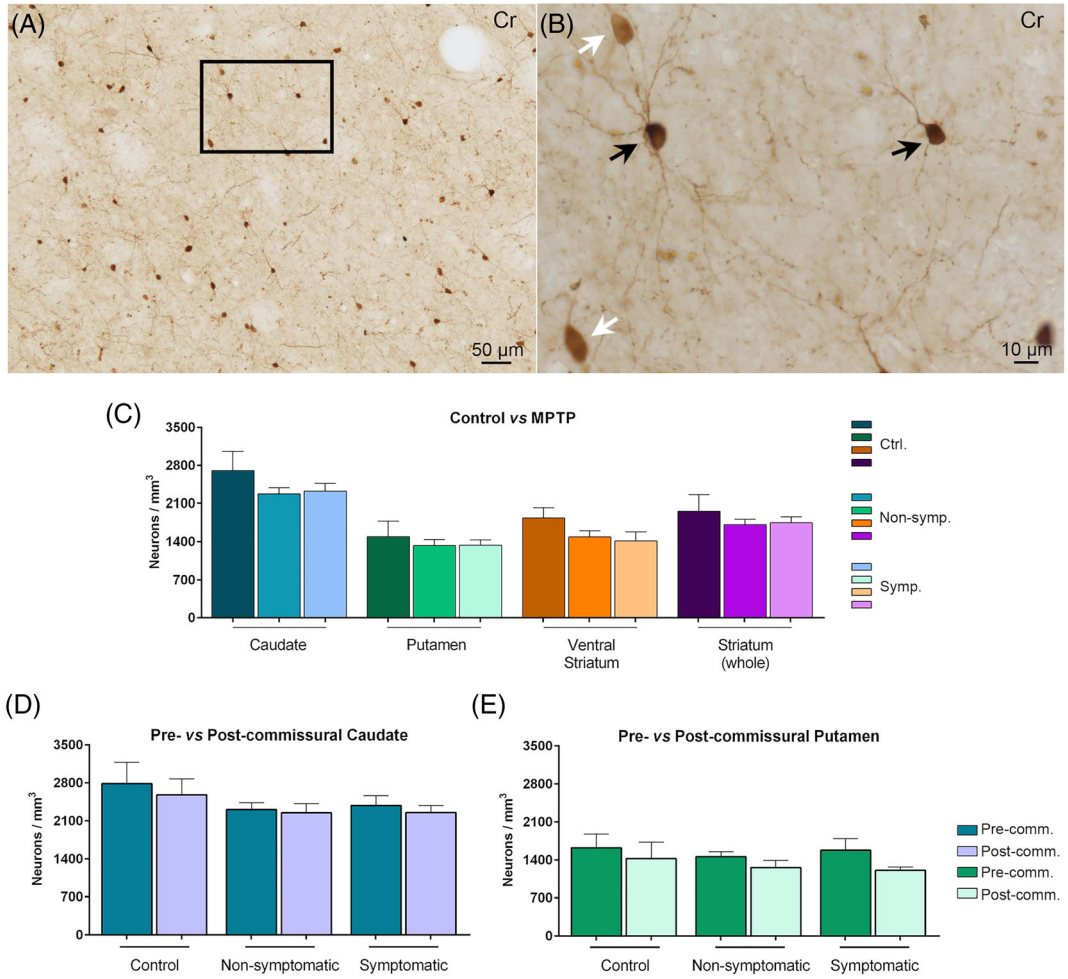

FIGURE 4 Cr+ neurons. (A and B) low magnification (10×) (A) and high magnification (40×) (B) photomicrographs of neurons expressing CR in a control monkey. The picture in (B) corresponds to the rectangle area in (A). Note that medium (white arrows) and intensely stained (black arrows) neurons are intermixed. (C) Densities of Cr+ neurons in the striatal nuclei of control and MPTP-treated monkeys; and densities in pre- and post-commissural caudate (D) and putamen (E) in each experimental group. No changes in Cr+ neuron densities were present in either striatal territory of the MPTP non-human primate model as compared with the control group

throughout the striatal nuclei (control 449 ± 9; non-symptomatic 402 ± 21; symptomatic 453 ± 13) ($p = 0.0845$) (Figure 6C–E).

ChAT+ neurons in control and MPTP-treated monkeys

ChAT+ interneurons were the largest of all striatal neurons, having average diameters of 23 µm and 14 µm (longest and shortest, respectively). In some ChAT+ neurons, the longest diameter reached up to 39 µm. ChAT+ neurons were intensively stained and were polygonal, with two to six principal dendrites (Table 2, Figure 7A,B). Overall, ChAT+ staining appeared homogeneous throughout the whole striatum (Figure 1).

There was a higher density of ChAT+ neurons in the ventral striatum (464 ± 44) than in the caudate (264 ± 13) and putamen (395 ± 34) in control monkeys (Figure 7C). This pattern was also present in the MPTP-treated monkeys (Figure 7C). ChAT+ interneurons were denser in the post-commissural putamen (control pre-commissural putamen 279 ± 32; control post-commissural putamen 469 ± 34) (Figure 7E). Densities of ChAT+ neurons were similar in the control and MPTP-treated groups throughout the whole striatum (control 344 ± 23; non-symptomatic 289 ± 15; symptomatic 331 ± 10) ($p = 0.737$) (Figure 7C–E).

TH+ neurons in control and MPTP-treated monkeys

TH+ neurons were the smallest interneurons; their average diameters were 9 µm and 6 µm (longest and shortest, respectively). They were morphologically oval or round, either unipolar or bipolar (Table 2, Figure 8A–D).

The overall TH+ neuropil staining pattern was homogeneous throughout the striatum; the ventral striatum was somewhat more

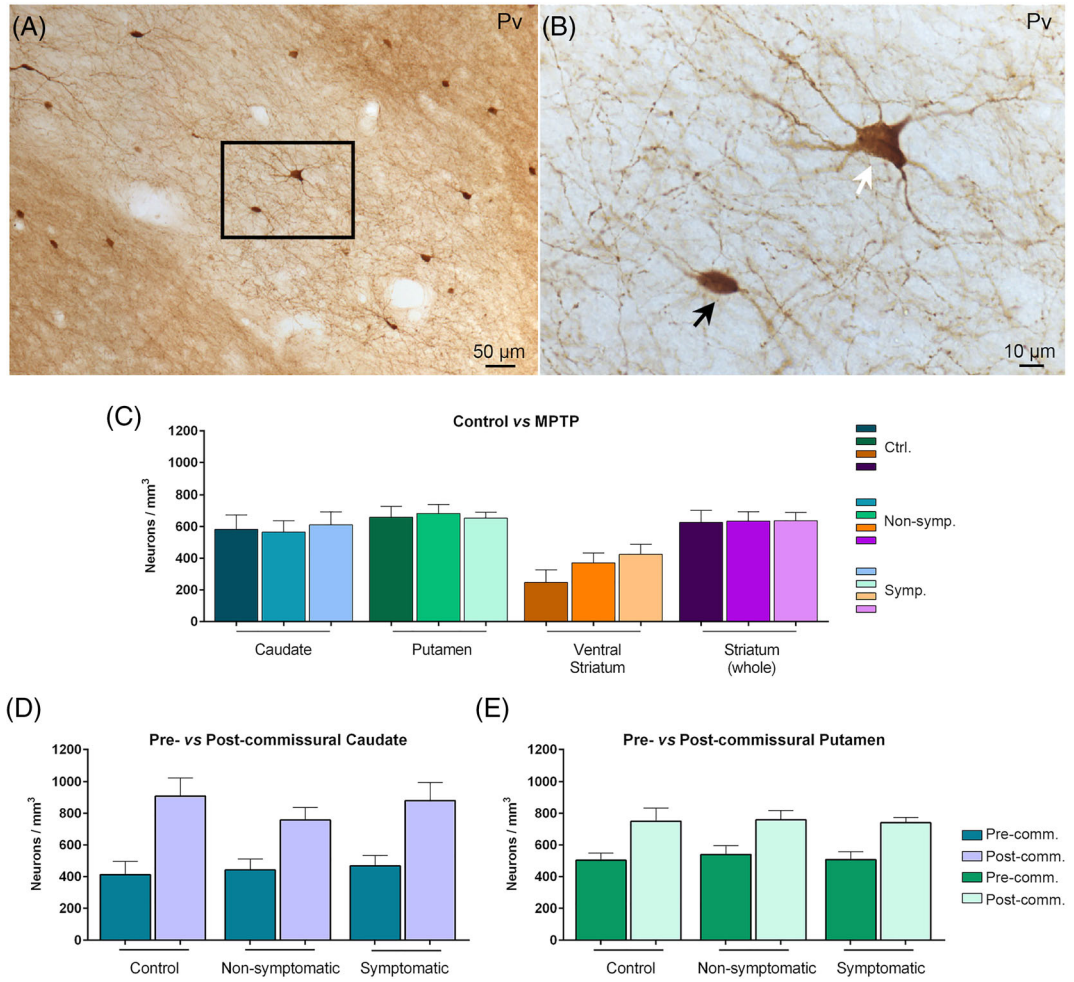

FIGURE 5 Pv+ neurons. (A and B) low magnification (10×) (A) and high magnification (40×) (B) photomicrographs of neurons expressing Pv in a control monkey. The picture in B corresponds to the rectangle area in a. note the presence of round bipolar and branched bigger neurons (black and white arrows, respectively). (C) Densities of Pv+ neurons in the striatal nuclei of control and MPTP-treated monkeys; and densities in pre- and post-commissural caudate (D) and putamen (E) in each experimental group. Lower Pv+ densities were found in the ventral striatum of control and MPTP-treated monkeys (C). Post-commissural Pv+ densities were higher in both caudate (D) and putamen (E) in all experimental groups

intensely stained. Also, patches of light TH staining were present in every section; they correspond to the striosomes (Figure 1), where the TH+ neuropil is less dense than in the surrounding matrix [52].

The neuron density was higher in the caudate (23 ± 2) than in the putamen (13 ± 2) of control monkeys; very few TH+ interneurons were observed in the ventral striatum (3 ± 3) (Figure 8E). Most TH+ neurons were located in the dorsal and dorsolateral caudate and putamen (Figure 8A).

In the MPTP-treated monkeys, in both non-symptomatic (29 ± 9; $p = 0.1453$) and symptomatic (37 ± 3; $p = 0.004$) animals, there was a higher density of TH+ neurons than in the control group (19 ± 1) throughout the whole striatum (Figure 8E). The increase of TH+ neuron density was also statistically significant in the caudate (43 ± 5; $p = 0.0246$) and putamen (28 ± 3; $p = 0.0384$) of the symptomatic group when compared with the control group (Figure 8E–G). An increase of TH+ neuron density was also present in the non-symptomatic group, but it was not statistically significant (caudate: 30 ± 3, $p = 0.8479$; putamen: 24 ± 3, $p = 0.1905$). In the MPTP-treated monkeys, the TH+ neurons were distributed in the dorsal and dorsolateral parts of both caudate and putamen, as in the control brains, but were additionally present in a more medial position in ventral and caudal striatum, especially in the putamen.

DISCUSSION

The present study shows that the projection neurons and the interneurons represent ~86% and ~14%, respectively, of the total neuron density in the adult macaque monkey striatum. Also, notable density differences are present in the interneuron populations, with the Cr+ neurons being the most abundant and the TH+ neurons the least (Cr+ > Pv+ > NADPH+ > ChAT+ > TH+). Interestingly, the percentages of projection neurons and interneurons remained unaffected in the DA-depleted striatum following MPTP treatment with the exception

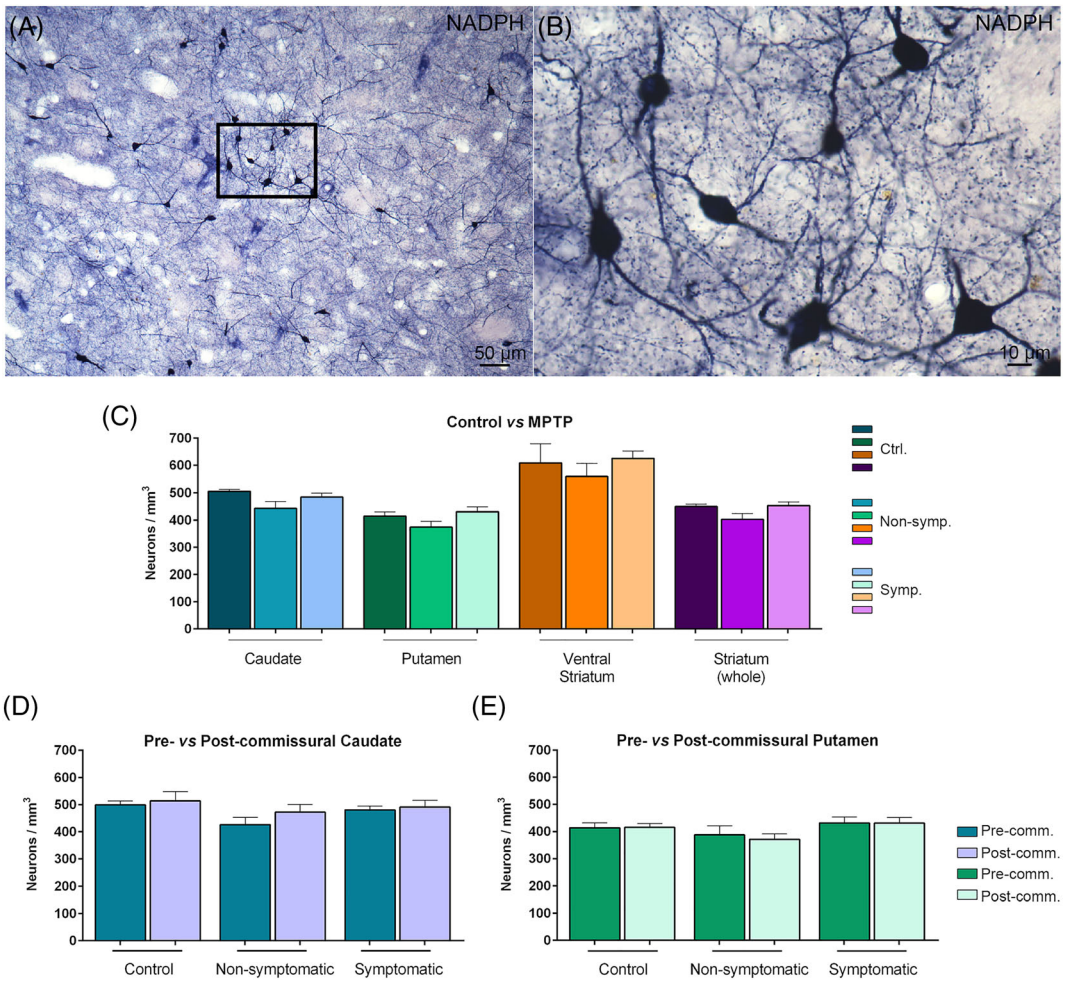

FIGURE 6 NADPH+ neurons. (A and B) low magnification (10×) (A) and high magnification (40×) (B) photomicrographs of neurons expressing NADPH in a control monkey. The picture in (B) corresponds to the rectangle area in (A). (C) Densities of NADPH+ neurons in the striatal nuclei of control and MPTP-treated monkeys; and densities in pre- and post-commissural caudate (D) and putamen (E) in each experimental group. No NADPH+ neuron density changes were present between the striatal territories in the parkinsonian stages (C–E)

of the TH+ population, which doubled in monkeys with severe striatal dopaminergic denervation (Figure 2).

The data presented here were obtained using state-of-the-art stereological analysis and encompassing the whole striatum as well as specific striatal territories (caudate, putamen, ventral striatum, pre-commissural and post-commissural striatum). Also, the neuron phenotypes analysed here do not co-localise [4] (the exception is a minor overlap, less than 1%, between Cr+ and ChAT+ neurons [53, 54]). It is possible that the striatal populations studied here may in turn include subpopulations. Indeed, additional neuron populations have been described, including, as an example, those expressing the ionotropic serotonin receptor 3 (5-HTR3a), secretagogin or the Kv3.3 potassium channel. However, most of these neurons are subpopulations of other striatal populations (Pv+, Cr+, TH+, neuropeptide Y+) [4, 55–59].

This is the first study analysing all neuron populations of the ventral and dorsal striatum in the same brains from both control and MPTP-treated macaques in diverse disease stages (non-symptomatic and symptomatic). Thus, accurate comparisons between interneuron populations can be made, as they come from the same subjects and analogous experimental and analysis methods are used. The finding that most neuron populations of the striatum endure DA depletion has implications for understanding the pathophysiology of the DA-depleted striatum and for designing therapeutic approaches in PD and parkinsonian conditions.

Interneurons in the healthy striatum

The present data show that interneurons make up ∼14% of all neuron types throughout the macaque monkey striatum. Reports over the last 30 years have provided quite diverse percentages of striatal interneurons ranging between 3%–5% in rodents, 5%–23% in monkeys and up to 11%–26% in humans [28, 30, 51]. Such wide-ranging differences in the data may result from different quantification methods (the earlier studies did not use stereological analysis) and from the use of

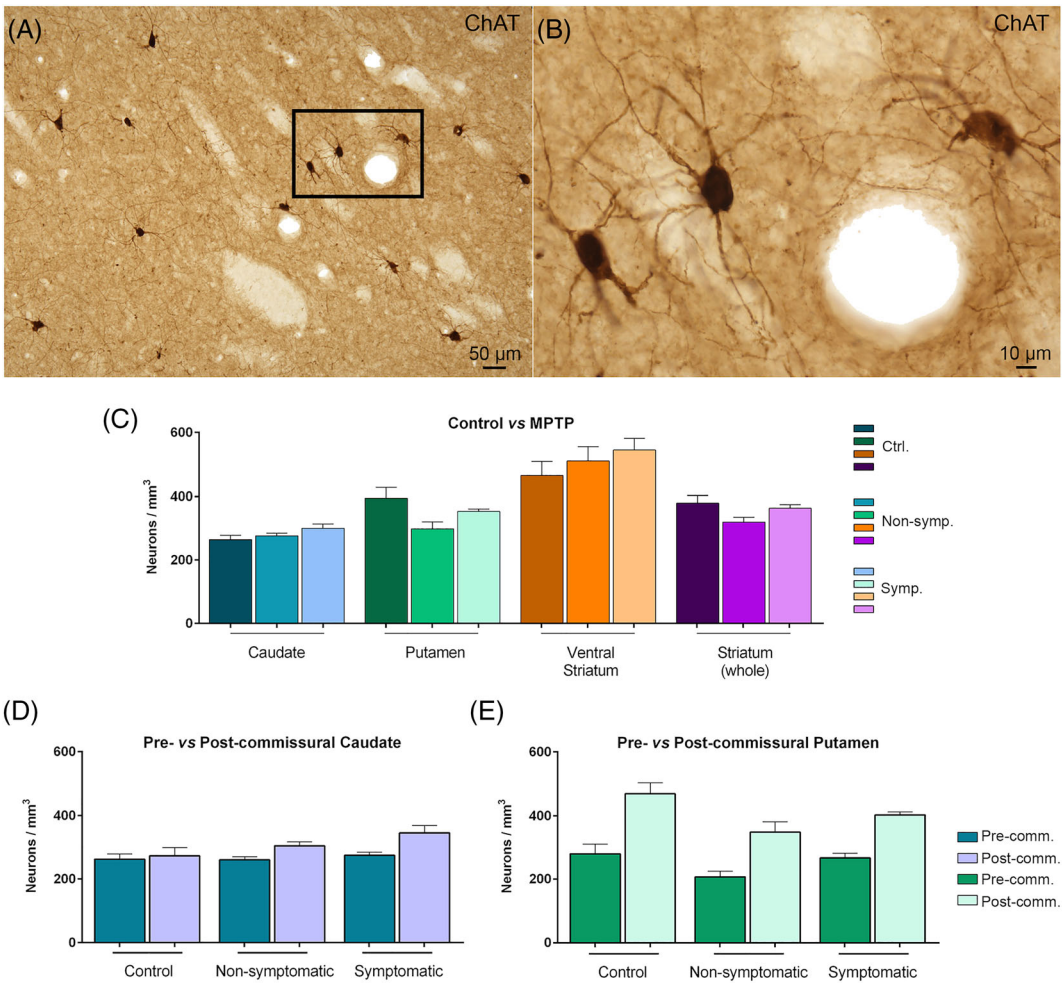

FIGURE 7 ChAT+ neurons. (A and B) low magnification (10×) (A) and high magnification (40×) (B) photomicrographs of neurons expressing ChAT in a control monkey. The picture in (B) corresponds to the rectangle area in (A). (C) Densities of ChAT+ neurons in the striatal nuclei of control and MPTP-treated monkeys; and densities in pre- and post-commissural caudate (D) and putamen (E) in each experimental group. Densities of ChAT+ neurons were lowest in the caudate (C). Higher densities of ChAT+ neurons were found in the post-commissural putamen as compared with the pre-commissural putamen

different phenotypic markers. For instance, calbindin striatal interneurons colocalize with both DARPP-32+ and with NADPH+ neurons [60, 61]. Calbindin immunostaining was omitted in the present study but was used in other studies [29, 51]. Here, we have used phenotypic markers that identify specific neuron populations of the primate and human striatum [4, 5]. Just a very minor percentage of the Cr+ neurons, the largest ones (~1.5% of the total Cr+ population in the present study, i.e., ~1 in 1000 striatal neurons), co-express ChAT [53, 62]. Thus, the current data, based on stereological analysis and a set of non-overlapping phenotypic markers, provide a solid estimation of the macaque striatal interneurons. Interestingly, the human striatum appears to contain percentages of striatal interneurons in the range of the non-human primate striatum [27, 30, 51]. Compared with rodents, the primate striatum has around three times more striatal interneurons, possibly reflecting notable interspecies differences in anatomical and connectional architectures.

The present study also provides the percentages, as well as volume densities, for each striatal interneuron population: 57% for Cr+, 18% for Pv+, 13% for NADPH+, 11% for ChAT+ and 0.5% for TH+ neurons (Figures 2–8). The exception to this ordered array of striatal interneurons lies in the ventral striatum, where the Pv+ population is less dense than the NADPH+ and ChAT+ populations (Figures 3–7). The densities of most interneurons are similar in the macaque caudate and putamen, either pre- or post-commissural. The exceptions are (1) the Cr+ interneurons, which are denser in the caudate than in the putamen; (2) the Pv+ interneurons, which are denser in the post-commissural caudate and putamen; and (3) the ChAT+ interneurons, which are denser in the post-commissural putamen (Figures 3–7). In the squirrel monkey and human striatum, the Cr+ interneurons are also the most abundant, followed by the Pv+ and NADPH+ [31, 63]. In contrast, in the rat striatum the populations of Cr+ and Pv+ interneurons are either similar [63] or the Pv+ interneurons are the most abundant [28]. Interspecies differences underline the importance of considering the relative presence of each neuron population to interpret striatal network changes in basal ganglia conditions of both humans and animal models.

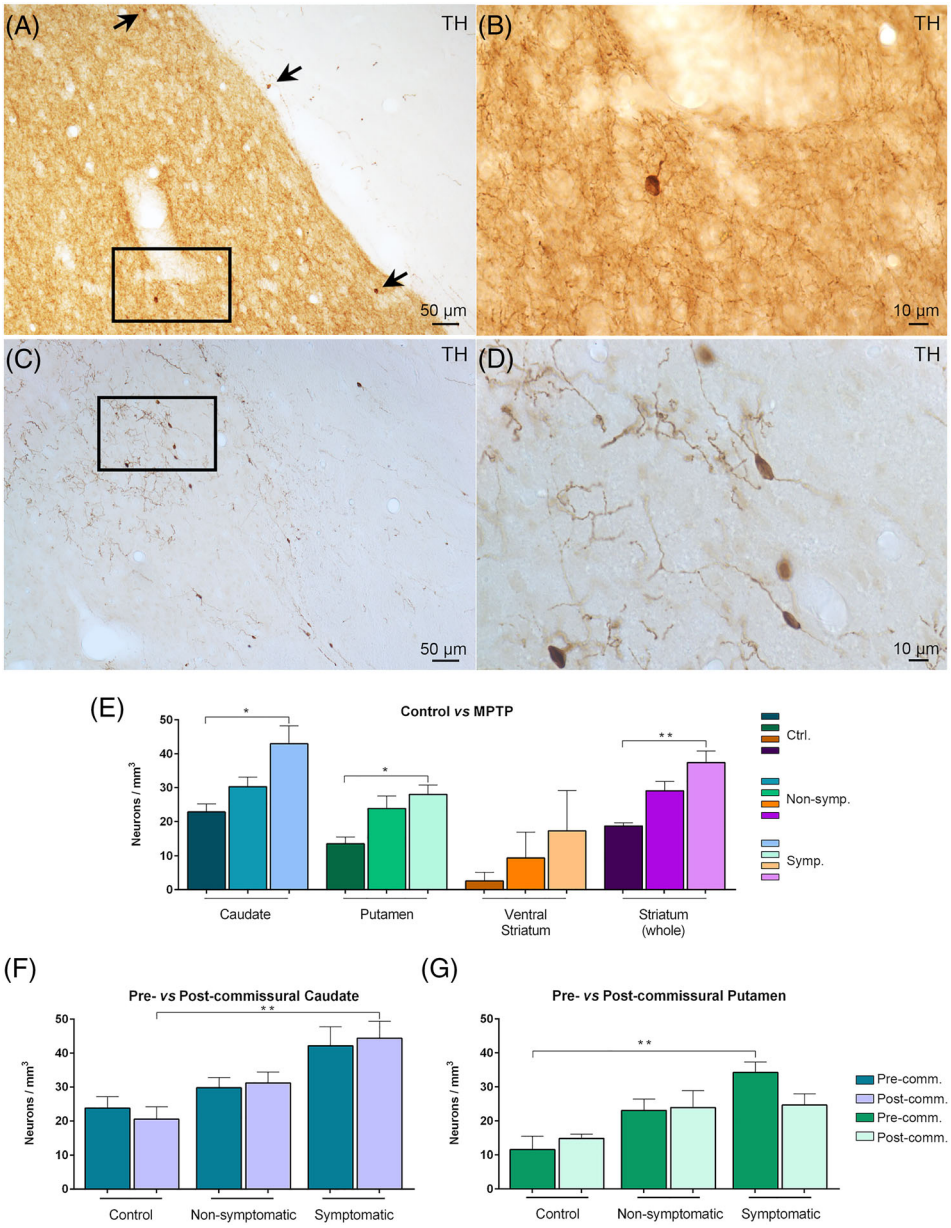

FIGURE 8 TH+ neurons. (A and B) low magnification (10×) (A) and high magnification (40×) (B) photomicrographs of neurons expressing TH from a control monkey. The arrows in (A) point to TH+ neuron bodies outside the rectangle area enlarged in (B). (C and D) low magnification (10×) (C) and high magnification (40×) (D) photomicrographs of neurons expressing TH from a MPTP-treated symptomatic monkey. The pictures in (B) and (D) correspond to the rectangle areas in (A) and (C), respectively. (E) Densities of TH+ neurons in the striatal nuclei of control and MPTP-treated monkeys; and densities in pre- and post-commissural caudate (F) and putamen (G) in each experimental group. Lower densities of TH+ neurons in ventral striatum were observed in comparison with other striatal nuclei (E). Significant changes in caudate, putamen and total striatum were found in the symptomatic group compared with control animals (F). Significance: $^{*}p < 0.05$; $^{**}p < 0.01$

Projection neurons and interneurons in the dopamine-depleted striatum

No significant changes in percentages or volume densities occur in any striatal neuron population following DA depletion, even massive depletion, except for the TH+ interneurons, which increase in the non-symptomatic subjects and even more in the symptomatic monkeys (Figures 2 and 8).

To our knowledge, this is the first quantitative study demonstrating the numerical stability of most striatal neuron populations, both the projection neurons (DARPP-32+) and the interneurons, in the DA-depleted striatum (Figure 2). Significantly, we have shown conspicuous axonal and neuron body changes, mostly loss, in the brains of the MPTP-treated monkeys used in the present study, particularly regarding the meso-striatal system [37] and the thalamic dopaminergic system [38]. The serotonin innervation of the striatum, however, did not change in the same brains [36]. Taking all factors into consideration, some brain systems are vulnerable and undergo marked changes following DA depletion, but others do not. The neuron populations of the striatum, both projection neurons and interneurons, survive the MPTP insult so that their densities remain stable. The TH+ neurons are the only exception as they increase in the DA-depleted striatum.

Earlier studies addressing the impact of DA depletion on the numbers of two specific striatal interneurons in primates have shown, in line with the present findings, that no major changes are present in the densities of striatal Cr+ and ChAT+ interneurons in MPTP-treated macaques [53, 64]. In rodents, however, opposite results regarding the Cr+ interneurons in the DA-depleted striatum have been published: transient increase [65] or a decrease [66, 67].

The caudate and putamen of DA-depleted symptomatic monkeys had about two times more TH+ interneurons than those of the control monkeys, a difference that was statistically significant. The functional impact of this finding should be considered in the context of the relative abundance and location of the TH+ interneurons: Their percentage in the macaque striatum is very low (from 0.54% to 1.17% in control and symptomatic parkinsonian monkeys, respectively). In addition, they are unevenly distributed: The TH+ neurons are very scant in the ventral striatum and concentrate in the dorsal and dorsolateral caudate and putamen (in the DA-depleted brains they are also present more centrally in those nuclei).

TH+ neurons are considered a specific population of striatal interneurons because they do not express markers of projection neurons or other interneuron populations in monkeys [68–70]. Our data on their size and morphologies also support that they are a specific interneuron population (Table 2). As to the co-expression of other markers by striatal TH+ neurons, there is agreement that they are GABAergic both in primates [68, 71] and in rodents [72–74]. Regarding DAT expression, there are conflicting results in the literature [68, 69, 71, 73]; it seems that TH+ neurons are not dopaminergic [73]. Interestingly, the distribution patterns of striatal TH+ interneurons differ between primates and rodents. While in primates they concentrate in the dorsal striatum (present data and earlier reports [31, 70]), in mice they are also present in the ventral striatum [75].

Manifold results have been published regarding the fate and significance of TH+ interneurons in diverse species. In PD patients, both increase [76] and decrease [71, 77] of TH+ striatal interneurons have been reported. The decrease was attributed to the fact that the patients had received L-DOPA treatment, which may restore DA striatal levels, as demonstrated in a pilot study in primates [78]. In parkinsonian animal models, however, increase in the number of TH+ striatal interneurons has been systematically documented in parallel to striatal DA depletion in a variety of models and species, including mice [74, 79–81], rats [82–84] and monkeys [68–70, 78, 85, 86]. It has been proposed that the increase in TH+ striatal neurons is the result of a phenotypic shift from pre-existing GABAergic interneurons [68]. A similar phenotypic shift has been proposed for the small population of large Cr+ interneurons in primates which would result from Cr expression in some ChAT+ neurons [53].

The functional role of striatal TH+ neurons has been investigated quite extensively in mice [4]. These neurons have been attributed a significant role in the transmission and distribution of neuromodulatory signals within the striatal circuitry [74]. They receive strong excitatory input from the cortex and thalamus [11, 72, 87], pointing to a specific engagement by different excitatory inputs. Also, selective ablation of striatal TH+ interneurons results in impaired goal-directed behaviour, while preserving motoric and appetitive behaviours [88]. In primates, the role of striatal TH+ neurons remains to be elucidated, both in normal and in pathological conditions.

Striatal neurons in Parkinson's disease and other neurodegenerative conditions

Loss of DA innervation in the striatum is causally and directly related with cardinal features of PD. Further, it is currently accepted that striatal interneurons are major determinants of network activity and behaviour in PD and L-DOPA-induced dyskinesia. Indeed, like projection neurons, all striatal interneurons express DA receptors, adding an extra dimension to the mechanisms of DA modulation of striatal activity and their impairment in PD and L-DOPA-induced dyskinesia [12, 15, 89–91]. The striatal interneurons also refine the networks engaging projection neurons and their cortical and thalamic inputs [9, 18]. Moreover, the functional effect of both cortical and thalamic inputs on the striatum greatly depends on the connectivity of the different types of striatal interneurons [11, 13, 92–94]. More precisely, the organisation of corticostriatal and thalamostriatal inputs relies on distinct striatal functional territories and on individual postsynaptic cell types [8, 9, 95]. In particular, striatal activity is dynamically modulated by acetylcholine and DA, both of which are essential for motor function [96, 97]. Accordingly, numerous recent studies have suggested that targeting ChAT+ interneurons in pharmacological intervention may improve motor dysfunction and L-DOPA induced dyskinesia in parkinsonism [10, 24, 89, 98–101]. Likewise, other interneuron populations have been suggested as a potential target to ameliorate parkinsonian signs: Pv+ interneurons, which synthesise most of the striatal glial cell line-derived neurotrophic factor (GDNF) [25, 102], and NADPH+ interneurons, whose inhibition has been suggested to attenuate L-DOPA induced dyskinesia [103].

The future development of specific drugs should allow efficient targeting of particular neuron populations [104], not just in PD, but also in various brain disorders, including Huntington's disease [26], Tourette's syndrome [105, 106] or addiction [107, 108]. The data presented here may help study and understand the cellular and functional impact of such interventions in the primate striatum.

Conclusion

The present study, based on an unbiased quantitative approach, provides data on the numerical volume densities and relative percentages of the projection and interneuron populations of the macaque striatum. The present data will be valuable for comparative studies on the striatal circuitry involving rodents, monkeys and humans. In addition, the finding that DA depletion does not alter the numbers of the striatal neuron populations (except for the meagre TH+) is relevant to understand the functional connectivity of striatal networks in the DA-depleted striatum and crucial for developing therapeutic interventions directed at striatal interneurons in PD.

ACKNOWLEDGEMENTS

The expert technical assistance with histology of Rosa Sánchez Lozano and Raquel Márquez López is gratefully acknowledged.

N.L.G, J.B. and J.A.O. are currently funded by Ministerio de Educación y Formación Profesional PID2019-111045RB-100 and grant S2017/BMD-3700 (NEUROMETAB-CM) from Comunidad de Madrid; J.B. by Instituto de Salud Carlos III Miguel Servet Program (CP19/00200) and FIS (PI20/00496); and C.C. by Chair in Neuroscience UAM-Fundación Tatiana Pérez de Guzmán el Bueno.

CONFLICT OF INTEREST

The authors declare no conflicts of interest.

ETHICS STATEMENT

All the studies were performed according to European and Spanish guidelines (86/609/EEC and 2003/65/EC European Council Directives; and Spanish Government) and were approved by the Committees for Research Ethics of the University of Navarra and Autónoma de Madrid University.

AUTHOR CONTRIBUTIONS

JAO, CC and JB designed the research; NLGR, ITD and JB performed the research; NLGR, CC and JB analysed the data and wrote the paper; all authors read and approved the final version of the manuscript.

DATA AVAILABILITY STATEMENT

The data that support the findings of this study are available from the corresponding author upon reasonable request.

ORCID

Natalia López-González del Rey https://orcid.org/0000-0002-1546-1825
Inés Trigo-Damas https://orcid.org/0000-0002-7821-2973
José A. Obeso https://orcid.org/0000-0002-6996-8613
Carmen Cavada https://orcid.org/0000-0001-7230-1388
Javier Blesa https://orcid.org/0000-0002-4257-1325

REFERENCES

1. Cox J, Witten IB. Striatal circuits for reward learning and decision-making. *Nat Rev Neurosci*. 2019;20(8):482-494. doi:10.1038/s41583-019-0189-2
2. Ouimet CC, Lamantia AS, Goldman-Rakic P, Rakic P, Greengard P. Immunocytochemical localization of DARPP-32, a dopamine and cyclic-AMP-regulated phosphoprotein, in the primate brain. *J Comp Neurol*. 1992;323(2):209-218. doi:10.1002/cne.903230206
3. Ouimet CC, Langley-Gullion KC, Greengard P. Quantitative immunocytochemistry of DARPP-32-expressing neurons in the rat caudatoputamen. *Brain Res*. 1998;808(1):8-12. doi:10.1016/S0006-8993(98)00724-0
4. Tepper JM, Koós T, Ibanez-Sandoval O, Tecuapetla F, Faust TW, Assous M. Heterogeneity and diversity of striatal GABAergic interneurons: update 2018. *Front Neuroanat*. 2018;12:91. doi:10.3389/fnana.2018.00091
5. Tepper JM, Tecuapetla F, Koós T, Ibáñez-Sandoval O. Heterogeneity and diversity of striatal GABAergic interneurons. *Front Neuroanat*. 2010;4:150. doi:10.3389/fnana.2010.00150
6. Muñoz-Manchado AB, Bengtsson Gonzales C, Zeisel A, et al. Diversity of interneurons in the dorsal striatum revealed by single-cell RNA sequencing and PatchSeq. *Cell Rep*. 2018;24(8):2179-2190.e7. doi:10.1016/j.celrep.2018.07.053
7. Xiao L, Bornmann C, Hatstatt-Burklé L, Scheiffele P. Regulation of striatal cells and goal-directed behavior by cerebellar outputs. *Nat Commun*. 2018;9(1):3133. doi:10.1038/s41467-018-05565-y
8. Johansson Y, Silberberg G. The functional organization of cortical and thalamic inputs onto five types of striatal neurons is determined by source and target cell identities. *Cell Rep*. 2020;30(4):1178-1194.e3. doi:10.1016/j.celrep.2019.12.095
9. Peters AJ, Fabre JMJ, Steinmetz NA, Harris KD, Carandini M. Striatal activity topographically reflects cortical activity. *Nature*. 2021;18(591):420-425. doi:10.1038/s41586-020-03166-8
10. Dautan D, Huerta-Ocampo I, Gut NK, et al. Cholinergic midbrain afferents modulate striatal circuits and shape encoding of action strategies. *Nat Commun*. 2020;11(1):1739. doi:10.1038/s41467-020-15514-3
11. Assous M, Kaminer J, Shah F, Garg A, Koós T, Tepper JM. Differential processing of thalamic information via distinct striatal interneuron circuits. *Nat Commun*. 2017;8(1):15860. doi:10.1038/ncomms15860
12. Dorst MC, Tokarska A, Zhou M, et al. Polysynaptic inhibition between striatal cholinergic interneurons shapes their network activity patterns in a dopamine-dependent manner. *Nat Commun*. 2020;11(1):5113. doi:10.1038/s41467-020-18882-y
13. Yoshida K, Tsutsui-Kimura I, Kono A, et al. Opposing ventral striatal medium spiny neuron activities shaped by striatal parvalbumin-expressing interneurons during goal-directed behaviors. *Cell Rep*. 2020;31(13):107829. doi:10.1016/j.celrep.2020.107829
14. Hjorth J, Kozlov A, Carannante I, et al. The microcircuits of striatum in silico. *Proc Natl Acad Sci U S A*. 2020;117(17):9554-9565. doi:10.1073/pnas.2000671117
15. Gritton HJ, Howe WM, Romano MF, et al. Unique contributions of parvalbumin and cholinergic interneurons in organizing striatal networks during movement. *Nat Neurosci*. 2019;22(4):586-597. doi:10.1038/s41593-019-0341-3
16. Silberberg G, Bolam JPP. Local and afferent synaptic pathways in the striatal microcircuitry. *Curr Opin Neurobiol*. 2015;33:182-187. doi:10.1016/j.conb.2015.05.002
17. Kocaturk S, Shah F, Guven B, Tepper JM, Assous M. Cholinergic control of striatal GABAergic microcircuits. *bioRxiv*. 2021. doi:10.1101/2021.11.22.469580
18. Plotkin JL, Goldberg JA. Thinking outside the box (and arrow): current themes in striatal dysfunction in movement disorders. *Neuroscientist*. 2019;25(4):359-379. doi:10.1177/1073858418807887
19. Lewis RG, Serra M, Radl D, et al. Dopaminergic control of striatal cholinergic interneurons underlies cocaine-induced psychostimulation. *Cell Rep*. 2020;31(3):107527. doi:10.1016/j.celrep.2020.107527
20. Zhai S, Shen W, Graves SM, Surmeier DJ. Dopaminergic modulation of striatal function and Parkinson's disease. *J Neural Transm*. 2019;126(4):411-422. doi:10.1007/s00702-019-01997-y
21. Friedman A, Hueske E, Drammis SM, et al. Striosomes mediate value-based learning vulnerable in age and a Huntington's disease model. *Cell*. 2020;183(4):918-934.e49. doi:10.1016/j.cell.2020.09.060
22. Cuzon Carlson VC, Gremel CM, Lovinger DM. Gestational alcohol exposure disrupts cognitive function and striatal circuits in adult offspring. *Nat Commun*. 2020;11(1):2555. doi:10.1038/s41467-020-16385-4
23. Vormstein-Schneider D, Lin JD, Pelkey KA, et al. Viral manipulation of functionally distinct interneurons in mice, non-human primates and humans. *Nat Neurosci*. 2020;23(12):1629-1636. doi:10.1038/s41593-020-0692-9
24. Choi SJ, Ma TC, Ding Y, et al. Alterations in the intrinsic properties of striatal cholinergic interneurons after dopamine lesion and chronic l-dopa. *Elife*. 2020;9:e56920. doi:10.7554/eLife.56920
25. Enterría-Morales D, del Rey NL-G, Blesa J, et al. Molecular targets for endogenous glial cell line-derived neurotrophic factor modulation

in striatal parvalbumin interneurons. *Brain Commun*. 2020;2(2): fcaa105. doi:10.1093/braincomms/fcaa105
26. Crevier-Sorbo G, Rymar VV, Crevier-Sorbo R, Sadikot AF. Thalamostriatal degeneration contributes to dystonia and cholinergic interneuron dysfunction in a mouse model of Huntington's disease. *Acta Neuropathol Commun*. 2020;8(1):14. doi:10.1186/s40478-020-0878-0
27. Graveland GA, Difiglia M. The frequency and distribution of medium-sized neurons with indented nuclei in the primate and rodent neostriatum. *Brain Res*. 1985;327(1-2):307-311. doi:10.1016/0006-8993(85)91524-0
28. Oorschot DE. The percentage of interneurons in the dorsal striatum of the rat, cat, monkey and human: a critique of the evidence. *Basal Ganglia*. 2013;3(1):19-24. doi:10.1016/j.baga.2012.11.001
29. Deng YP, Shelby E, Reiner AJ. Immunohistochemical localization of AMPA-type glutamate receptor subunits in the striatum of rhesus monkey. *Brain Res*. 2010;1344:104-123. doi:10.1016/j.brainres.2010.05.003
30. Krienen FM, Goldman M, Zhang Q, et al. Innovations present in the primate interneuron repertoire. *Nature*. 2020;586(7828):262-269. doi:10.1038/s41586-020-2781-z
31. Bernácer J, Prensa L, Giménez-Amaya JM. Distribution of GABAergic interneurons and dopaminergic cells in the functional territories of the human striatum. *PLoS ONE*. 2012;7:e30504. doi:10.1371/journal.pone.0030504
32. Roberts RC, Gaither LA, Peretti FJ, Lapidus B, Chute DJ. Synaptic organization of the human striatum: a postmortem ultrastructural study. *J Comp Neurol*. 1996;374(4):523-534. doi:10.1002/(SICI)1096-9861(19961028)374:4%3C523::AID-CNE4%3E3.0.CO;2-3
33. Graveland GA, Williams RS, Difiglia M. A Golgi study of the human neostriatum: neurons and afferent fibers. *J Comp Neurol*. 1985;234(3):317-333. doi:10.1002/cne.902340304
34. Bernácer J, Prensa L, Giménez-Amaya JMM, Bernacer J, Prensa L, Gimenez-Amaya JM. Cholinergic interneurons are differentially distributed in the human striatum. *PLoS ONE*. 2007;2(11):e1174. doi:10.1371/journal.pone.0001174
35. Figueredo-Cardenas G, Morello M, Sancesario G, Bernardi G, Reiner A. Colocalization of somatostatin, neuropeptide Y, neuronal nitric oxide synthase and NADPH-diaphorase in striatal interneurons in rats. *Brain Res*. 1996;735(2):317-324. doi:10.1016/0006-8993(96)00801-3
36. Jiménez-Sánchez L, Blesa J, Del Rey NL, Monje MHG, Obeso JA, Cavada C. Serotonergic innervation of the striatum in a nonhuman primate model of Parkinson's disease. *Neuropharmacology*. 2020;170:107806. doi:10.1016/j.neuropharm.2019.107806
37. Blesa J, Pifl C, Sánchez-González MA, et al. The nigrostriatal system in the presymptomatic and symptomatic stages in the MPTP monkey model: a PET, histological and biochemical study. *Neurobiol Dis*. 2012;48(1):79-91. doi:10.1016/j.nbd.2012.05.018
38. Monje MHG, Blesa J, García-Cabezas MÁ, Obeso JA, Cavada C. Changes in thalamic dopamine innervation in a progressive Parkinson's disease model in monkeys. *Mov Disord*. 2020;35(3):419-430. doi:10.1002/mds.27921
39. Blesa J, Juri C, Collantes M, et al. Progression of dopaminergic depletion in a model of MPTP-induced Parkinsonism in non-human primates: an (18)F-DOPA and (11)C-DTBZ PET study. *Neurobiol Dis*. 2010;38(3):456-463. doi:10.1016/j.nbd.2010.03.006
40. Liu C, Goel P, Kaeser PS. Spatial and temporal scales of dopamine transmission. *Nat Rev Neurosci*. 2021;22(6):345-358. doi:10.1038/s41583-021-00455-7
41. Blesa J, Juri C, García-Cabezas MÁ, et al. Inter-hemispheric asymmetry of nigrostriatal dopaminergic lesion: a possible compensatory mechanism in Parkinson's disease. *Front Syst Neurosci*. 2011;5:92. doi:10.3389/fnsys.2011.00092
42. Kurlan R, Kim MHH, Gash DMM. The time course and magnitude of spontaneous recovery of parkinsonism produced by intracarotid administration of 1-methyl-4-phenyl-1,2,3,6-tetrahydropyridine to monkeys. *Ann Neurol*. 1991;29(6):677-679. doi:10.1002/ana.410290618
43. Cavada C, Compañy T, Hernández-González A, et al. Acetylcholinesterase histochemistry in the macaque thalamus reveals territories selectively connected to frontal, parietal and temporal association cortices. *J Chem Neuroanat*. 1995;8(4):245-257. doi:10.1016/0891-0618(95)00050-H
44. Matamales M, Bertran-Gonzalez J, Salomon L, et al. Striatal medium-sized spiny neurons: identification by nuclear staining and study of neuronal subpopulations in BAC transgenic mice. *PLoS ONE*. 2009;4(3):e4770. doi:10.1371/journal.pone.0004770
45. Bertran-Gonzalez J, Bosch C, Maroteaux M, et al. Opposing patterns of signaling activation in dopamine D1 and D2 receptor-expressing striatal neurons in response to cocaine and haloperidol. *J Neurosci*. 2008;28(22):5671-5685. doi:10.1523/JNEUROSCI.1039-08.2008
46. Hope BT, Vincent SR. Histochemical characterization of neuronal NADPH-diaphorase. *J Histochem Cytochem*. 1989;37(5):653-661. doi:10.1177/37.5.2703701
47. Gundersen HJG, Jensen EBV, Kiêu K, Nielsen J. The efficiency of systematic sampling in stereology—reconsidered. *J Microsc*. 1999;193(3):199-211. doi:10.1046/j.1365-2818.1999.00457.x
48. Keuker JIH, Vollmann-Honsdorf GK, Fuchs E. How to use the optical fractionator: an example based on the estimation of neurons in the hippocampal CA1 and CA3 regions of tree shrews. *Brain Res Protoc*. 2001;7(3):211-221. doi:10.1016/S1385-299X(01)00064-2
49. Dorph-Petersen KA, Nyengaard JR, Gundersen HJG. Tissue shrinkage and unbiased stereological estimation of particle number and size. *J Microsc*. 2001;204(3):232-246. doi:10.1046/j.1365-2818.2001.00958.x
50. Carlo CN, Stevens CF. Analysis of differential shrinkage in frozen brain sections and its implications for the use of guard zones in stereology. *J Comp Neurol*. 2011;519(14):2803-2810. doi:10.1002/cne.22652
51. Lecumberri A, Lopez-Janeiro A, Corral-Domenge C, Bernacer J. Neuronal density and proportion of interneurons in the associative, sensorimotor and limbic human striatum. *Brain Struct Funct*. 2018;223(4):1615-1625. doi:10.1007/s00429-017-1579-8
52. Graybiel AMM, Ragsdale CW. Histochemically distinct compartments in the striatum of human, monkeys, and cat demonstrated by acetylthiocholinesterase staining. *Proc Natl Acad Sci U S A*. 1978;75(11):5723-5726. 10.1073/pnas.75.11.5723
53. Petryszyn S, Di Paolo T, Parent A, Parent M. The number of striatal cholinergic interneurons expressing calretinin is increased in parkinsonian monkeys. *Neurobiol Dis*. 2016;95:46-53. doi:10.1016/j.nbd.2016.07.002
54. Cicchetti F, Beach TG, Parent A. Chemical phenotype of calretinin interneurons in the human striatum. *Synapse*. 1998;30(3):284-297. doi:10.1002/(SICI)1098-2396(199811)30:3%3C284::AID-SYN6%3E3.0.CO;2-7
55. Faust TW, Assous M, Shah F, Tepper JM, Koós T. Novel fast adapting interneurons mediate cholinergic-induced fast GABAA inhibitory postsynaptic currents in striatal spiny neurons. *Eur J Neurosci*. 2015;42(2):1764-1774. doi:10.1111/ejn.12915
56. Assous M, Faust TW, Assini R, Shah F, Sidibe Y, Tepper JM. Identification and characterization of a novel spontaneously active bursty GABAergic interneuron in the mouse striatum. *J Neurosci*. 2018;38(25):5688-5699. doi:10.1523/JNEUROSCI.3354-17.2018
57. Muñoz-Manchado AB, Foldi C, Szydlowski S, et al. Novel striatal GABAergic interneuron populations labeled in the 5HT3a(EGFP) mouse. *Cereb Cortex*. 2016;26(1):96-105. doi:10.1093/cercor/bhu179

58. Garas FN, Shah RS, Kormann E, et al. Secretagogin expression delineates functionally-specialized populations of striatal parvalbumin-containing interneurons. *Elife*. 2016;5:e16088 10.7554/eLife.16088
59. Lebenheim L, Booker SA, Derst C, et al. A novel giant non-cholinergic striatal interneuron restricted to the ventrolateral striatum coexpresses Kv3.3 potassium channel, parvalbumin, and the vesicular GABA transporter. *Mol Psychiatry*. 2020. doi:10.1038/s41380-020-00948-4
60. Kawaguchi Y, Wilson CJ, Augood SJ, Emson PC. Striatal interneurons—chemical, physiological and morphological characterization. *Trends Neurosci*. 1995;18(12):527-535. doi:10.1016/0166-2236(95)98374-8
61. Bennett BD, Bolam JP. Two populations of calbindin D28k-immunoreactive neurones in the striatum of the rat. *Brain Res*. 1993;610(2):305-310. doi:10.1016/0006-8993(93)91414-N
62. Petryszyn S, Parent A, Parent M. The calretinin interneurons of the striatum: comparisons between rodents and primates under normal and pathological conditions. *J Neural Transm*. 2018;125(3):279-290. doi:10.1007/s00702-017-1687-x
63. Wu Y, Parent A. Striatal interneurons expressing calretinin, parvalbumin or NADPH-diaphorase: a comparative study in the rat, monkey and human. *Brain Res*. 2000;863(1-2):182-191. doi:10.1016/S0006-8993(00)02135-1
64. Villalba RMM, Pare J-FF, Lee S, Smith Y. Thalamic degeneration in MPTP-treated Parkinsonian monkeys: impact upon glutamatergic innervation of striatal cholinergic interneurons. *Brain Struct Funct*. 2019;224(9):3321-3338. doi:10.1007/s00429-019-01967-w
65. Mura A, Feldon J, Mintz M. The expression of the calcium binding protein calretinin in the rat striatum: effects of dopamine depletion and L-DOPA treatment. *Exp Neurol*. 2000;164(2):322-332. doi:10.1006/exnr.2000.7441
66. Petryszyn S, Saidi L, Gagnon D, Parent A, Parent M. The density of calretinin striatal interneurons is decreased in 6-OHDA-lesioned mice. *Brain Struct Funct*. 2021;226(6):1879-1891. doi:10.1007/s00429-021-02298-5
67. Ma Y, Feng Q, OuYang L, et al. Morphological diversity of GABAergic and cholinergic interneurons in the striatal dorsolateral and ventromedial regions of rats. *Cell Mol Neurobiol*. 2014;34(3):351-359. doi:10.1007/s10571-013-0019-4
68. Tandé D, Höglinger G, Debeir T, Freundlieb N, Hirsch ECC, François C. New striatal dopamine neurons in MPTP-treated macaques result from a phenotypic shift and not neurogenesis. *Brain*. 2006;129(5):1194-1200. doi:10.1093/brain/awl041
69. Betarbet R, Turner R, Chockkan V, et al. Dopaminergic neurons intrinsic to the primate striatum. *J Neurosci*. 1997;17(17):6761-6768. doi:10.1523/JNEUROSCI.17-17-06761.1997
70. Mazloom M, Smith Y. Synaptic microcircuitry of tyrosine hydroxylase-containing neurons and terminals in the striatum of 1-methyl-4-phenyl-1,2,3,6-tetrahydropyridine- treated monkeys. *J Comp Neurol*. 2006;495(4):453-469. doi:10.1002/cne.20894
71. Huot P, Lévesque M, Parent A. The fate of striatal dopaminergic neurons in Parkinson's disease and Huntington's chorea. *Brain*. 2007;130(Pt 1):222-232. doi:10.1093/brain/awl332
72. Ibáñez-Sandoval O, Tecuapetla F, Unal B, et al. Electrophysiological and morphological characteristics and synaptic connectivity of tyrosine hydroxylase-expressing neurons in adult mouse striatum. *J Neurosci*. 2010;30(20):6999-7016. doi:10.1523/JNEUROSCI.5996-09.2010
73. Xenias HSS, Ibanez-Sandoval O, Koos T, et al. Are striatal tyrosine hydroxylase interneurons dopaminergic? *J Neurosci*. 2015;35(16):6584-6599. doi:10.1523/JNEUROSCI.0195-15.2015
74. Ibáñez-Sandoval O, Xenias HSS, Tepper JMM, Koós T. Dopaminergic and cholinergic modulation of striatal tyrosine hydroxylase interneurons. *Neuropharmacology*. 2015;95:468-476. doi:10.1016/j.neuropharm.2015.03.036
75. Unal B, Ibáñez-Sandoval O, Shah F, Abercrombie ED, Tepper JM. Distribution of tyrosine hydroxylase-expressing interneurons with respect to anatomical organization of the neostriatum. *Front Syst Neurosci*. 2011;5:41. doi:10.3389/fnsys.2011.00041
76. Porritt MJ, Batchelor PE, Hughes AJ, Kalnins R, Donnan GA, Howells DW. New dopaminergic neurons in Parkinson's disease striatum. *Lancet*. 2000;356(9223):44-45. doi:10.1016/S0140-6736(00)02437-5
77. Porritt MJ, Kingsbury AE, Hughes AJ, Howells DW. Striatal dopaminergic neurons are lost with Parkinson's disease progression. *Mov Disord*. 2006;21(12):2208-2211. doi:10.1002/mds.21129
78. Huot P, Lévesque M, Morissette M, et al. L-Dopa treatment abolishes the numerical increase in striatal dopaminergic neurons in parkinsonian monkeys. *J Chem Neuroanat*. 2008;35(1):77-84. doi:10.1016/j.jchemneu.2007.06.004
79. Busceti CL, Bucci D, Molinaro G, et al. Lack or inhibition of dopaminergic stimulation induces a development increase of striatal tyrosine hydroxylase-positive interneurons. *PLoS ONE*. 2012;7(9):e44025. doi:10.1371/journal.pone.0044025
80. Darmopil S, Muñetón-Gómez VC, De Ceballos ML, Bernson M, Moratalla R. Tyrosine hydroxylase cells appearing in the mouse striatum after dopamine denervation are likely to be projection neurones regulated by L-DOPA. *Eur J Neurosci*. 2008;27(3):580-592. doi:10.1111/j.1460-9568.2008.06040.x
81. Espadas I, Darmopil S, Vergaño-Vera E, et al. L-DOPA-induced increase in TH-immunoreactive striatal neurons in parkinsonian mice: insights into regulation and function. *Neurobiol Dis*. 2012;48(3):271-281. doi:10.1016/j.nbd.2012.07.012
82. Meredith GE. Immunocytochemical characterization of catecholaminergic neurons in the rat striatum following dopamine-depleting lesions. *Eur J Neurosci*. 1999;11(10):3585-3596. doi:10.1046/j.1460-9568.1999.00774.x
83. Lopez-Real A, Rodriguez-Pallares J, Guerra MJ, Labandeira-Garcia JL. Localization and functional significance of striatal neurons immunoreactive to aromatic L-amino acid decarboxylase or tyrosine hydroxylase in rat Parkinsonian models. *Brain Res*. 2003;969(1-2):135-146. doi:10.1016/S0006-8993(03)02291-1
84. Tashiro Y, Sugimoto T, Hattori T, et al. Tyrosine hydroxylase-like immunoreactive neurons in the striatum of the rat. *Neurosci Lett*. 1989;97(1-2):6-10. doi:10.1016/0304-3940(89)90130-4
85. Palfi S, Leventhal L, Chu Y, et al. Lentivirally delivered glial cell line-derived neurotrophic factor increases the number of striatal dopaminergic neurons in primate models of nigrostriatal degeneration. *J Neurosci*. 2002;22(12):4942-4954. doi:10.1523/JNEUROSCI.22-12-04942.2002
86. Huot P, Parent A. Dopaminergic neurons intrinsic to the striatum. *J Neurochem*. 2007;101(6):1441-1447. doi:10.1111/j.1471-4159.2006.04430.x
87. Assous M, Tepper JM. Cortical and thalamic inputs exert cell type-specific feedforward inhibition on striatal GABAergic interneurons. *J Neurosci Res*. 2019;97(12):1491-1502. doi:10.1002/jnr.24444
88. Kaminer J, Espinoza D, Bhimani S, Tepper JM, Koos T, Shiflett MW. Loss of striatal tyrosine-hydroxylase interneurons impairs instrumental goal-directed behavior. *Eur J Neurosci*. 2019;50(4):2653-2662. doi:10.1111/ejn.14412
89. Shen W, Ren W, Zhai S, et al. Striatal Kir2 K+ channel inhibition mediates the antidyskinetic effects of amantadine. *J Clin Invest*. 2020;130(5):2593-2601. doi:10.1172/JCI133398
90. Gittis AH, Hang GB, LaDow ES, et al. Rapid target-specific remodeling of fast-spiking inhibitory circuits after loss of dopamine. *Neuron*. 2011;71(5):858-868. doi:10.1016/j.neuron.2011.06.035
91. Lee K, Holley SM, Shobe JL, et al. Parvalbumin interneurons modulate striatal output and enhance performance during associative learning. *Neuron*. 2017;93(6):1451-1463.e4. doi:10.1016/j.neuron.2017.02.033

92. Klug JR, Engelhardt MD, Cadman CN, et al. Differential inputs to striatal cholinergic and parvalbumin interneurons imply functional distinctions. *Elife*. 2018;7:e35657. doi:10.7554/eLife.35657
93. Mamaligas AA, Barcomb K, Ford CP. Cholinergic transmission at muscarinic synapses in the striatum is driven equally by cortical and thalamic inputs. *Cell Rep*. 2019;28(4):1003-1014.e3. doi:10.1016/j.celrep.2019.06.077
94. Holly EN, Davatolhagh MF, Choi K, Alabi OO, Cifuentes LV, Fuccillo MV. Striatal low-threshold spiking interneurons regulate goal-directed learning. *Neuron*. 2019;103(1):92-101.e6. doi:10.1016/j.neuron.2019.04.016
95. Fino E, Vandecasteele M, Perez S, Saudou F, Venance L. Region-specific and state-dependent action of striatal GABAergic interneurons. *Nat Commun*. 2018;9(1):1-17. doi:10.1038/s41467-018-05847-5
96. Maurice N, Liberge M, Jaouen F, et al. Striatal cholinergic interneurons control motor behavior and basal ganglia function in experimental parkinsonism. *Cell Rep*. 2015;13(4):657-666. doi:10.1016/j.celrep.2015.09.034
97. Albaugh DL, Gittis AH. Stressing the importance of cholinergic interneurons in striatal function. *Mov Disord*. 2021;37:36.
98. McKinley JW, Shi Z, Kawikova I, et al. Dopamine deficiency reduces striatal cholinergic interneuron function in models of Parkinson's disease. *Neuron*. 2019;103(6):1056-1072.e6. doi:10.1016/j.neuron.2019.06.013
99. Tanimura A, Du Y, Kondapalli J, Wokosin DL, Surmeier DJ. Cholinergic interneurons amplify thalamostriatal excitation of striatal indirect pathway neurons in Parkinson's disease models. *Neuron*. 2019;101(3):444-458.e6. doi:10.1016/j.neuron.2018.12.004
100. Lozovaya N, Eftekhari S, Cloarec R, et al. GABAergic inhibition in dual-transmission cholinergic and GABAergic striatal interneurons is abolished in Parkinson disease. *Nat Commun*. 2018;9(1):1422. doi:10.1038/s41467-018-03802-y
101. Assous M. Striatal cholinergic transmission. Focus on nicotinic receptors' influence in striatal circuits. *Eur J Neurosci*. 2021;53(8):2421-2442. doi:10.1111/ejn.15135
102. Duarte Azevedo M, Sander S, Jeanneret C, Olfat S, Tenenbaum L. Selective targeting of striatal parvalbumin-expressing interneurons for transgene delivery. *J Neurosci Methods*. 2021;354:109105. doi:10.1016/j.jneumeth.2021.109105
103. Padovan-Neto FE, Cavalcanti-Kiwiatkoviski R, Carolino ROG, Anselmo-Franci J, Del Bel E. Effects of prolonged neuronal nitric oxide synthase inhibition on the development and expression of l-DOPA-induced dyskinesia in 6-OHDA-lesioned rats. *Neuropharmacology*. 2015;89:87-99. doi:10.1016/j.neuropharm.2014.08.019
104. Lerchner W, Adil AA, Mumuney S, et al. RNAi and chemogenetic reporter co-regulation in primate striatal interneurons. *Gene Ther*. 2021;29(1-2):69-80. doi:10.1038/s41434-021-00260-y
105. Xua M, Kobetsa A, Dua JC, et al. Targeted ablation of cholinergic interneurons in the dorsolateral striatum produces behavioral manifestations of Tourette syndrome. *Proc Natl Acad Sci U S A*. 2015;112(3):893-898. doi:10.1073/pnas.1419533112
106. Lennington JB, Coppola G, Kataoka-Sasaki Y, et al. Transcriptome Analysis of the Human Striatum in Tourette Syndrome. *Biol Psychiatry*. 2016;79(5):372-382. doi:10.1016/j.biopsych.2014.07.018
107. Schall TA, Wright WJ, Dong Y. Nucleus accumbens fast-spiking interneurons in motivational and addictive behaviors. *Mol Psychiatry*. 2021;26(1):234-246. doi:10.1038/s41380-020-0683-y
108. Clarke R, Adermark L. Dopaminergic regulation of striatal interneurons in reward and addiction: focus on alcohol. *Neural Plast*. 2015;2015:814567. doi:10.1155/2015/814567

SUPPORTING INFORMATION

Additional supporting information may be found in the online version of the article at the publisher's website.

How to cite this article: del Rey NL-G, Trigo-Damas I, Obeso JA, Cavada C, Blesa J. Neuron types in the primate striatum: Stereological analysis of projection neurons and interneurons in control and parkinsonian monkeys. *Neuropathol Appl Neurobiol*. 2022;e12812. doi:10.1111/nan.12812